J Electr Eng Technol.2018; 13(4): 1515-1527
http://doi.org/10.5370/JEET.2018.13.4.1515

ISSN(Print) 1975-0102
ISSN(Online) 2093-7423

Sensorless Control of IPMSM with a Simplified High-Frequency Square Wave Injection Method

Ahmadreza Alaei*, Dong-Hee Lee, Jin-Woo Ahn† and Sayed Morteza Saghaeian Nejad***

Abstract – This paper presents a sensorless speed control of IPMSM (Interior Permanent Magnet Synchronous Motor) using the high-frequency (HF) square wave injection method. In the proposed HF pulsating square wave injection method, injection voltage is applied into the estimated d-axis of rotor and high-frequency induced q-axis current is considered to estimate the rotor position. Conventional square wave injection methods may need complex demodulation process to find rotor position, while in the proposed method, an easy demodulation process based on the rising-falling edge of the injected voltage and carrier induced q-axis current is implemented, which needs less processing time and improves control bandwidth. Unlike some saliency-based sensorless methods, the proposed method uses maximum torque per ampere (MTPA) strategy, instead of zero d-axis command current strategy, to improve control performance. Furthermore, this paper directly uses resultant d-axis current to detect the magnet polarity and eliminates the need to add an extra pulse injection for magnet polarity detection. As experimental results show, the proposed method can quickly find initial rotor position and MTPA strategy helps to improve the control performance. The effectiveness of the proposed method and all theoretical concepts are verified by mathematical equations, simulation, and experimental tests.

Keywords: IPMSM(interior permanent magnet synchronous motor), Sensorless control, Square wave voltage injection, Rotor position estimation, MTPA(maximum torque per ampere), Magnet polarity detection

1. Introduction

Nowadays, permanent magnet synchronous motors (PMSMs) are used widely in many applications and industries due to some merits such as high efficiency, high torque density, and fast dynamic response to load disturbance conditions. To achieve every PMSM capabilities, it is necessary to know the accurate rotor position, and therefore utilization of the position sensors such as encoders or resolvers is unavoidable. However, the position sensors not only increase the cost, but they also simultaneously increase the system weight, volume, drive circuit complexity, and decrease the whole system reliability. Therefore, sensorless control of PMSM has been researched and investigated over many years [1-4].

Basically, the sensorless drive algorithms can be divided into standstill and low-speed operation methods according to machine saliency and medium and high-speed regions based on the Back-Electromotive Force (BEMF). A lot of BEMF-based sensorless techniques are used mostly in the middle and high-speed regions, such as model reference adaptive system (MRAS), sliding mode observer (SMO), and extended Kalman filter (EKF). However, these methods become useless in the standstill-low speed regions due to the lack of BEMF at zero/low-speed values [5-8]. The BEMF based sensorless methods can be used for all types of PMSMs, including surface mounted permanent magnet synchronous motors (SPMSM) and interior permanent magnet synchronous motors (IPMSM) in the medium and high-speed range. On the other hands, for standstill and low-speed region, some High-Frequency (HF) signal injection sensorless techniques based on the machine saliency have been investigated [1, 5, 8-15]. It is proven that the rotor position information can be extracted from the negative sequence carrier current or zero sequence carrier voltage due to the high-frequency injection voltage on the stator windings [11, 16-18]. The resultant carrier current or voltage of the HF injection methods is a function of the machine saliency values and rotor position error. So, these techniques can be used for IPM synchronous machines which have inductance saliency and its performance degraded for SPM types.

HF signal injection methods in terms of injection signal shape are classified into sinusoidal wave injection and square wave injection methods. Sinusoidal voltage injection methods are classified into three popular methods: rotating signal injection in the stationary reference frame, pulsating signal injection in the estimated synchronous reference frame, and anti-clockwise pulsating injection in the estimated synchronous frame which rotates in reverse at

† Corresponding Author: Dept. of Mechatronics Engineering, Kyungsung University, Busan, Korea. (jwahn@ks.ac.kr)
* Dept. of Electrical Engineering, Isfahan University of Technology, Isfahan, Iran. (ahmadrezaalaei@gmail.com, saghaian@cc.iut.ac.ir)
** Dept. of Mechatronics Engineering, Kyungsung University, Busan, Korea. (leedh@ks.ac.kr)
Received: September 5, 2017; Accepted: January 26, 2018

twice of the rotor electrical speed [19]. It is proven that HF pulsating injection methods based on carrier current sensing have more advantages compared to the rotating injection, in terms of bandwidth enhancement and stability [20]. Also, it is proven that HF injection method based on zero sequence voltage is independent to the injection frequency, which results in higher injected frequency and bandwidth enhancement [8]. The anti-clockwise pulsating injection method based on zero sequence voltage sensing is more suitable because the advantages of the zero sequence voltage sensing method are combined with the pulsating injection method [21, 22]. However, in order to measure the zero-sequence voltage, one extra A/D converter channel and an access to the machine neutral point are necessary [14, 23].

Although HF sinusoidal injection methods are easier to implement, these methods suffered from low-frequency injection due to limited PWM frequency to make the HF sinusoidal wave [12]. In contrast, the square wave signal injection methods have the capability to increase the injection frequency which results in the bandwidth enhancement since there are no bandpass and low pass filters [8]. Although the square wave injection methods have more benefits compared to the sine wave injection types, these methods increase iron losses and acoustic noises due to an increase in voltage amplitude when high-frequency injection signal is required [19]. Furthermore, conventional square wave injection method may need a complex demodulation process done in a very short time to find the rotor position which may be sensitive to the current measurement noise [8, 11, 12].

This paper presented a high-frequency square wave signal injection technique based on current sensing method and maximum torque per ampere strategy (MTPA) which increases the bandwidth of HF signal injection based sensorless algorithms, due to the utilization of square wave injection. In this method, the required phase currents are measured at the PWM time interval, in which the ADC unit is synchronized with the PWM unit. The maximum torque per ampere strategy based on the q-axis current command and electrical torque equation is also used to improve control performance. Moreover, a simple technique is used to find the magnet polarity which is important in the initial state of PM machine. The theoretical concept of the proposed HF injection method is described firstly. Then, the performance of the proposed method is evaluated in MATLAB and through experiment tests. A prototype IPM synchronous motor is used to verify the effectiveness of the proposed sensorless algorithms in the experiment.

2. Analysis of High-Frequency Injection Method

2.1 Mathematical model of IPMSM

The dynamic model of an IPMSM can be described as,

$$\begin{bmatrix} v_q \\ v_d \end{bmatrix} = \begin{bmatrix} r_s + L_{sq}p & -\omega_e L_{sd} \\ \omega_e L_{sq} & r_s + L_{sd}p \end{bmatrix} \begin{bmatrix} i_q \\ i_d \end{bmatrix} + \begin{bmatrix} 0 \\ \omega_e \psi_m \end{bmatrix} \quad (1)$$

where r_s is the phase resistance andL_{sd}, L_{sq} are d-q self-inductances of the stator windings respectively. p is the derivative operator and $\psi_m$is the permanent magnet flux. v_q, v_d and i_q, i_d are d-q stator voltages and currents in the synchronous reference frame, respectively. ω_e is the rotor electrical velocity. For high-frequency injection based sensorless methods at stand-still and low-speed regions, BEMF can be neglected and cross-coupling term is also small thus it can also be ignored. With these assumptions, Eq. (1) can be simplified and presented as an inductive load equation [19]-[10]

$$\begin{bmatrix} v_q^h \\ v_d^h \end{bmatrix} = \begin{bmatrix} X_q^h & 0 \\ 0 & X_d^h \end{bmatrix} \begin{bmatrix} i_q^h \\ i_d^h \end{bmatrix} \quad (2)$$

where index h denotes the "High-Frequency."

2.2 Pulsating SIGNAL INJECTION MODEL

Fig. 1 shows the pulsating square wave voltage injection techniques in two-axis coordinate. $\hat{d}-\hat{q}$ indexes indicate the estimated synchronous reference frame, $d-q$ indexes indicate the actual synchronous reference frame, and $\alpha-\beta$ indexes denote the stationary reference frame. The θ_e and $\hat{\theta}_e$ are the actual and estimated electrical rotor position, respectively. In PMSM, d-q flux linkages in the stationary reference frame can be written as,

$$\begin{bmatrix} \lambda_\beta \\ \lambda_\alpha \end{bmatrix} = \begin{bmatrix} L_{sum} + L_{dif}\cos 2\theta_r & -L_{dif}\sin 2\theta_r \\ -L_{dif}\sin 2\theta_r & L_{sum} - L_{dif}\cos 2\theta_r \end{bmatrix} \begin{bmatrix} i_\beta \\ i_\alpha \end{bmatrix} \quad (3)$$

where $L_{sum} = \frac{Ls_d + Ls_q}{2}$, $L_{dif} = \frac{Ls_d - Ls_q}{2}$ are average and differential inductances, i_α, i_β and $\lambda_\alpha, \lambda_\beta$ are currents and flux linkages in the stationary reference frame, respectively.

The high frequency α-β current components can be driven from (3) and described as,

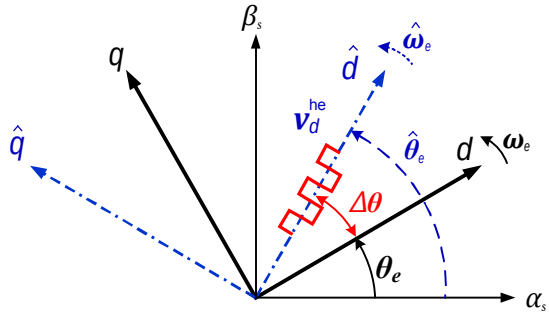

Fig. 1. Coordinate reference frame for HF pulsating square wave injection in the estimated synchronous reference frame

$$\begin{bmatrix} i_\beta^h \\ i_\alpha^h \end{bmatrix} = \frac{1}{\mathrm{Det(L)}} \begin{bmatrix} L_{sum} - L_{dif}\cos 2\theta_e & L_{diff}\sin 2\theta_e \\ L_{dif}\sin 2\theta_e & L_{sum} + L_{dif}\cos 2\theta_e \end{bmatrix} \begin{bmatrix} \lambda_\beta^h \\ \lambda_\alpha^h \end{bmatrix} \quad (4)$$

where Det (L) = $L_{sum}^2 - L_{dif}^2$. To develop the pulsating signal injection method in the estimated synchronous reference frame, Eq. (4) can be transferred to the estimated synchronous reference frame by using park transformation as,

$$\begin{bmatrix} i_q^{he} \\ i_d^{he} \end{bmatrix} = \begin{bmatrix} \cos 2\hat{\theta}_e & -\sin 2\hat{\theta}_e \\ \sin 2\hat{\theta}_e & \cos 2\hat{\theta}_e \end{bmatrix} \begin{bmatrix} i_\beta^h \\ i_\alpha^h \end{bmatrix} \quad (5)$$

where i_q^{he}, i_d^{he} are high-frequency d-q current components in the estimated synchronous reference frame. By substituting (5) into (4) and doing the simplification process, the resultant carrier currents in the estimated synchronous reference frame which includes the rotor position information can be extracted as,

$$\begin{bmatrix} i_q^{he} \\ i_d^{he} \end{bmatrix} = \frac{L_{sum}}{\det(L)} \begin{bmatrix} \lambda_q^{he} \\ \lambda_d^{he} \end{bmatrix} + \frac{L_{dif}}{\det(L)} \begin{bmatrix} -\cos(2\theta_e - 2\hat{\theta}_e) & \sin(2\theta_e - 2\hat{\theta}_e) \\ \sin(2\theta_e - 2\hat{\theta}_e) & \cos(2e - 2\hat{\theta}_e) \end{bmatrix} \begin{bmatrix} \lambda_q^{he} \\ \lambda_d^{he} \end{bmatrix} \quad (6)$$

Eq. (6) is valid for all types of the permanent magnet synchronous motors, either IPM or SPM synchronous types. It should be noted that for SPMSM types, L_{dif} is almost zero since L_d and L_q have the same values, approximately. On the other hand, high-frequency d-q flux linkage components in the estimated synchronous reference frame can be replaced by voltage equations as,

$$\begin{bmatrix} \lambda_q^{he} \\ \lambda_d^{he} \end{bmatrix} = \int \left(\begin{bmatrix} v_q^{he} \\ v_d^{he} \end{bmatrix} \right) dt \quad (7)$$

where v_q^{he}, v_d^{he} are the injected voltage in the estimated synchronous d-q axes and $\int() dt$ indicates the integration operator. By instituting (7) in (6), the basic equation for high frequency pulsating injection method is concluded as,

$$\begin{bmatrix} i_q^{he} \\ i_d^{he} \end{bmatrix} = \frac{L_{sum}}{\det(L)} \int \left(\begin{bmatrix} v_q^{he} \\ v_d^{he} \end{bmatrix} \right) dt + \frac{L_{dif}}{\det(L)} \begin{bmatrix} -\cos(2\theta_e - 2\hat{\theta}_e) & \sin(2\theta_e - 2\hat{\theta}_e) \\ \sin(2\theta_e - 2\hat{\theta}_e) & \cos(2\theta_e - 2\hat{\theta}_e) \end{bmatrix} \int \left(\begin{bmatrix} v_q^{he} \\ v_d^{he} \end{bmatrix} \right) dt \quad (8)$$

Eq. (8) can be used for both of sinusoidal voltage injection and square voltage injection methods. To evaluate the validity of Eq. (8), it is analyzed as an example for pulsating sinusoidal voltage injection method. For sinusoidal pulsating injection method, the injected voltage in the estimated d-axis is as shown in [16],

$$\begin{bmatrix} v_q^{he} \\ v_d^{he} \end{bmatrix} = v_i \begin{bmatrix} 0 \\ \cos w_h t \end{bmatrix} \quad (9)$$

By substituting (9) into (8), the difference between the actual rotor position and the estimated rotor position can be extracted from the resultant q-axis current as,

$$\begin{bmatrix} i_q^{he} \\ i_d^{he} \end{bmatrix} = \frac{v_i L_{sum}}{w_h \det(L)} \begin{bmatrix} 0 \\ \sin w_h t \end{bmatrix} + \frac{v_i L_{dif}}{w_h \det(L)} \begin{bmatrix} -\cos(2\theta_e - 2\hat{\theta}_e) & \sin(2\theta_e - 2\hat{\theta}_e) \\ \sin(2\theta_e - 2\hat{\theta}_e) & \cos(2\theta_e - 2\hat{\theta}_e) \end{bmatrix} \begin{bmatrix} 0 \\ \sin w_h t \end{bmatrix} \quad (10)$$

Therefore, from (10) it can be driven that,

$$i_q^{he} = \frac{v_i L_{dif}}{w_h \det(L)} \sin(2\theta_e - 2\hat{\theta}_e) \sin w_h t \quad (11)$$

By using the demodulation process and low pass filter, it concludes that,

$$I_q^{he} = \mathrm{LPF}(i_q^{he} * 2 \sin w_h t) = \frac{v_i L_{dif}}{w_h \det(L)} \sin(\Delta\theta) \quad (12)$$

where $\Delta\theta = 2(\theta_e - \hat{\theta}_e)$. It is proven that Eq. (12) is valid for HF sinusoidal pulsating injection method in the estimated synchronous reference frame [15]. Then, the position error function, i.e., I_q^{he}, is inserted into the rotor position observer and the rotor position can be extracted.

3. Proposed Pulsating Square Wave Signal Injection Method

3.1 Sensorless position estimation

Although sinusoidal HF signal injection methods are easy to implement, these methods suffered from a low-frequency injection because the PWM switching frequency is limited [8]. In this section, the principle of the proposed square wave injection method is illustrated and the MTPA algorithm is also described. Square wave pulsating injection method can be implemented by using a square wave voltage instead of sinusoidal voltage signal as,

$$\begin{bmatrix} v_q^{he} \\ v_d^{he} \end{bmatrix} = v_i \begin{bmatrix} 0 \\ \pm 1 \end{bmatrix} \quad (13)$$

Through substitution of (13) into the basic Eq. (8), the basic equation for the square wave voltage injection can be obtained as,

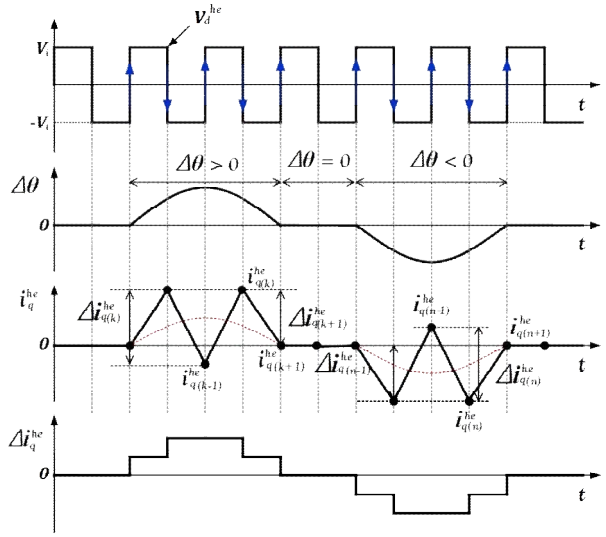

Fig. 2. Injection voltage on d-axis and resultant current on q-axis

$$\begin{bmatrix} i_q^{he} \\ i_d^{he} \end{bmatrix} = \frac{v_i\, L_{sum}}{det(L)} \begin{bmatrix} 0 \\ \pm t \end{bmatrix} + \frac{v_i\, L_{dif}}{det(L)} \begin{bmatrix} -\cos(2\theta_e - 2\hat{\theta}_e) & \sin(2\theta_e - 2\hat{\theta}_e) \\ \sin(2\theta_e - 2\hat{\theta}_e) & \cos(2\theta_e - 2\hat{\theta}_e) \end{bmatrix} \begin{bmatrix} 0 \\ \pm t \end{bmatrix} \quad (14)$$

where $\pm t$ in (14) is produced by the integration operator. By considering the q-axis current as the induced carrier current, the rotor position information is extracted as,

$$\begin{cases} i_q^{he} = \dfrac{v_i\, L_{dif}}{det(L)} \sin(2\theta_e - 2\hat{\theta}_e)t \quad \text{for } v_{di}^e > 0 \\ i_q^{he} = \dfrac{v_i\, L_{dif}}{det(L)} \sin(2\theta_e - 2\hat{\theta}_e)(-t) \text{ for } v_{di}^e < 0 \end{cases} \quad (15)$$

By considering the injected voltage as shown in Fig. 2, Eq. (15) can be written as,

$$\begin{cases} i_q^{he} = \dfrac{v_i\, L_{dif}}{det(L)} \dfrac{1}{Ti/2} \sin\Delta\theta\,.\,t \quad 0 < t < \dfrac{T_i}{2} \\ i_q^{he} = \dfrac{v_i\, L_{dif}}{det(L)} \dfrac{1}{T_i/2} \sin\Delta\theta\,(T_i - t) \quad \dfrac{T_i}{2} < t < T_i \end{cases} \quad (16)$$

where T_i is the sampling period of the injection voltage. The carrier induced currents in (16), which are used for rotor position estimation, have derivation process which increases the time processing consumption for demodulation. Besides that, the derivation of the carrier current is sensitive to the current measurement noises when the time interval is very short [8]. However, the proposed method uses the differentiation operator only at the specified points of PWM period. From $t = 0$ until $t = \frac{T_i}{2}$, the positive voltage is applied to the estimated d-axis. Using a differentiation operator at the falling edge of the injected voltage, (16) can be written as,

$$\begin{aligned} \Delta i_q^{he} &= i_q^{he}\left(t = \frac{T_i}{2}\right) - i_q^{he}(t = 0) \\ &\approx \frac{v_i\, L_{dif}}{det(L)} \frac{1}{Ti/2} \sin\Delta\theta\,.\frac{T_i}{2} \end{aligned} \quad (17)$$

From $t = \frac{T_i}{2}$ until $t = T_i$, the negative voltage is applied to estimated d-axis, therefore Δi_{qh}^e is calculated at the rising edge of the injected voltage and it is calculated as,

$$\begin{aligned} \Delta i_q^{he} &= i_q^{he}\left(t = \frac{T_i}{2}\right) - i_q^{he}(t = T_i) \\ &= \frac{v_i\, L_{dif}}{det(L)} \frac{1}{\frac{Ti}{2}} \sin\Delta\theta\,.\left(\frac{T_i}{2}\right) \end{aligned} \quad (18)$$

It should be noted that (17) is obtained at the falling edge of the injected voltage and (18) is also calculated at the rising edge of the injected voltage. Moreover, the rising and falling edge of the injection voltage in the sensorless algorithm is already known and is not necessary to detect. Therefore, the q-axis current difference can be calculated easily when the positive or negative voltage is injected to the estimated d-axis.

As can be seen from (17) and (18), the difference of HF q-axis current, Δi_{qh}^e, is proportional to the rotor position error without considering the sign of the injected voltage or any extra demodulation process, which results in a fast calculation of the position error. In almost all motor drives, the current sampling frequency of the ADC converter is synchronized with the PWM switching frequency. If $T_i = 2nT_{pwm}$ and $1 = \frac{v_i L_{dif}}{det(L)} \frac{1}{\frac{Ti}{2}}$, then (17) and (18) can be simplified as,

$$\begin{cases} \Delta i_q^{he} = k1.\Delta\theta.nT_{pwm} \quad 0 < t < nT_{pwm} \\ \Delta i_q^{he} = k1.\Delta\theta.nT_{pwm} \quad nT_{pwm} < t < 2nT_{pwm} \end{cases} \quad (19)$$

where T_{PWM} is the PWM time interval and n is the number of PWM cycle in one T_i period. It should be noted that the position error function, $\sin\Delta\theta$, is equal to $\Delta\theta$ approximately when the position error is small enough. So, for positive rotor position error ($\Delta\theta > 0$), it can be concluded that,

$$\begin{cases} for\ 0 < t < nT_{pwm}, \\ \Delta i_q^{he} = k1.|\Delta\theta|.nT_{pwm} \geq 0 \quad , v_{dh}^e > 0 \\ for\ nT_{pwm} < t < 2nT_{pwm}, \\ \Delta i_q^{he} = k1.|\Delta\theta|.nT_{pwm} \geq 0 \quad , v_{di}^e < 0 \end{cases} \quad (20)$$

For negative position error ($\Delta\theta < 0$), (20) can be rewritten as,

$$\begin{cases} for\ 0 < t < nT_{pwm}, \\ \Delta i_q^{he} = -k1.|\Delta\theta|.nT_{pwm} \le 0, \quad v_{dh}^e > 0 \\ for\ nT_{pwm} < t < 2nT_{pwm}, \\ \Delta i_q^{he} = -k1.|\Delta\theta|.nT_{pwm} \le 0, \quad v_{dh}^e < 0 \end{cases} \tag{21}$$

where $|\Delta\theta|$ is the absolute value of the position error. As can be observed from (20) and (21), the rotor position error is just a function of the carrier q-axis current difference. To highlight the position error function, table 1 is introduced based on the injected square wave voltage and the induced carrier q-axis current. As can be observed from the table 1, position error function is related to the rotor position error which can be inserted into the rotor position observer. Using rotor position observers such as PID controller or phase lock loop (PLL) observer, the estimated rotor position and velocity are extracted.

Fig.3 shows how the rotor position and velocity are obtained. The high-frequency q-axis current is measured and synchronized by PWM switching frequency which is determined by coefficient n. Δi_q^{he} is calculated at the rising and falling edge of the injection voltage. Utilizing a simple PID controller, the position error is forced to be zero and therefore, rotor position and velocity can be extracted.

3.2 Magnet polarity detection

Detection of the initial rotor position and polarity of the magnet is very important in all types of PMSM drive, whether it is sensorless or position sensor based drive. To find the initial rotor position in the standstill state, the HF square wave voltage is injected into the estimated d-axis of the rotor whereas the current commands for current loop controller are set to zero. Although the initial rotor position can be extracted by using the position estimator block based on the proposed HF square wave injection method, the estimated rotor position is ambiguous at 0 and π radian since the motor inductance function has the same values at these points. Therefore, one magnet polarity detection algorithm should be implemented to specify the rotor magnet polarity.

There exist a lot of research on the magnet polarity detection algorithms and therefore, further magnet polarity identification methods can be used [24, 25]. However, in this paper, a simple magnet polarity detection is also introduced based on d-axis current measurement. It should be noted that the proposed method uses the square wave injection for both rotor position estimation and magnet polarity detection, resulting in a fast sensorless startup which is beneficial in the sensorless drive. When the positive injection signal is applied to the north pole, i.e +vdh , the resultant stator flux, i.e, PM flux and injection flux are gathered, which results in more stator teeth saturation. Meanwhile, the negative injected voltage, i.e -vdh , results in lower stator teeth saturation. By considering the d-axis resultant current as a stator flux component, the magnet polarity can be distinguished by accumulating the peak value of the positive d-axis current in a certain period of time [13]. However, this method needs to measure the high-frequency d-axis current and accumulate the positive and negative number of the peak values, which may be sensitive to the current measurement noise.

The proposed magnet polarity detection method uses the low-frequency component of the d-axis current which is shown in Fig. 4. If the electrical rotor position is located between 0 ~ π rad, d-axis current slightly has positive values. In this situation, differentiation of the d-axis current has a positive slope which can be used for magnet polarity detection. For rotor position between π ~ 2π, d-axis current slightly has negative values compared to the position $0<\theta e<\pi$. Also, the slope of the differentiation of the d-axis current is negative. This phenomenon occurred due to the air gap flux which is augmented when the injected voltage is positive in the north pole and diminished when the injected voltage is negative on the south pole. After the initial rotor position was estimated by the position estimation block, the polarity-enabled flag enables the polarity detection algorithm for the specified time. Using the proposed method mentioned above, the magnet polarity is distinguished. When the initial rotor position was estimated, the rotor alignment flag is set and then, speed loop is activated. It should be noted that the offset in current sensing method has a bad effect on the magnet polarity detection in the initial rotor finding process,

Table 1. Rotor position error as a function of q-axis current difference (+refer to positive value and – vice versa)

$\Delta\theta$	Rising-Falling edge	Δi_q^{he}	Time	Position error function $\triangleq \Delta i_q^{he}$
+	↑	+	$0 < t < \frac{T_i}{2}$	+
+	↓	+	$\frac{T_i}{2} < t < T_i$	+
−	↑	−	$0 < t < \frac{T_i}{2}$	−
−	↓	−	$\frac{T_i}{2} < t < T_i$	−

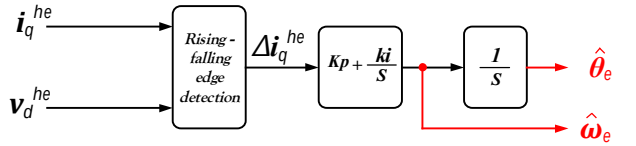

Fig. 3. Electrical rotor position and speed estimation based on the proposed method

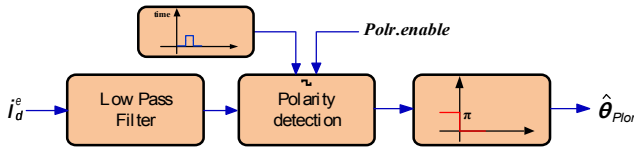

Fig. 4. Proposed magnet polarity detection at the initial drive startup

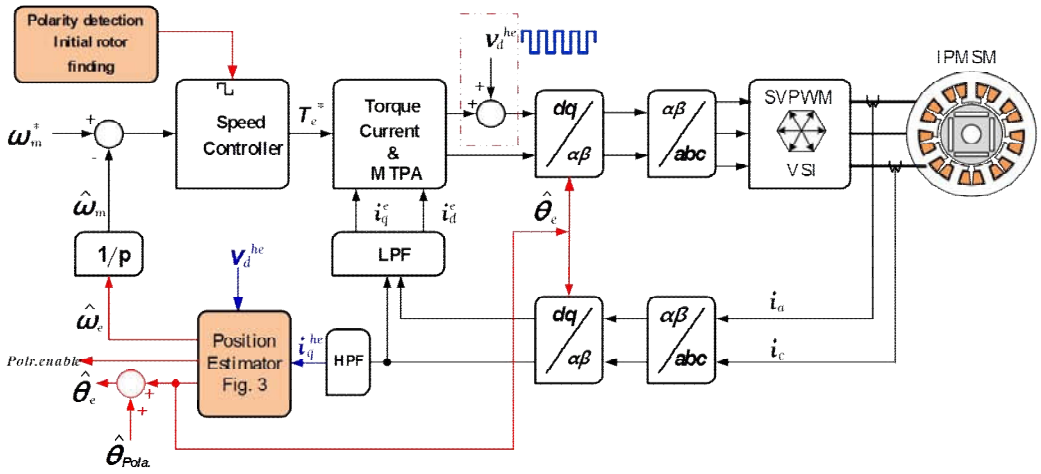

Fig. 5. Overall block diagram of the square wave voltage injection method for IPMSM sensorless drive

which is removed by using the high pass filter on the measured currents. Fig. 5 shows the overall control block diagram of the proposed high-frequency pulsating square wave injection method used in IPMSM sensorless drive. Speed control loop generates the command torque which produces d-q axis currents references according to the maximum torque per ampere strategy which is described as follows.

3.3 Maximum torque per ampere strategy

In most high-frequency injection methods, the strategy of the zero d-axis current, i.e. , $i_d^* = 0$ is used to control the d-axis flux [8]. In [9], the authors focused on the magnetic saturation effect on the machine saliency, taking into account the chosen current control strategy. However, by using the MTPA strategy, the resultant torque is increased and the machine performance is also increased, consequently. In the proposed HF square wave injection method, a simple MTPA strategy based on the torque equation in IPM synchronous machine is used to improve the performance of the HF injection based sensorless drive. In IPM synchronous machine, the total driven torque includes two components: the first one is the electromagnetic torque caused by the rotor magnetic flux and q-axis current interaction, and the next one is the reluctance torque caused by the interaction between the machine saliency and the d-q axis currents. Generally, the total driven torque in IPM synchronous motor can be described as,

$$T_t = \frac{3}{2}p(\psi_f i_q + (Ls_d - Ls_q) i_d i_q) \tag{22}$$

where ψ_f is the magnet flux linkage. To obtain the maximum torque per ampere conditions, the stator current constraint is considered as,

$$i_d^2 + i_q^2 \le is_n^2 \tag{23}$$

where is_n is the rated current of the motor. The maximum value of the q-axis current is calculated as,

$$i_q^2 = is_n^2 - i_d^2 \tag{24}$$

By substituting (24) into (22), the torque equation can be described as,

$$T_t = \frac{3}{2}p(\psi_f\sqrt{is_n^2 - i_d^2} + (Ls_d - Ls_q) i_d \sqrt{is_n^2 - i_d^2}) \tag{25}$$

To find the d-axis current in which the IPM total driven torque reaches to the maximum value, the derivative operation is declared as $\frac{dT_t}{di_d} = 0$. It means that,

$$\frac{3}{2}p\left(-\psi_f i_d + (Ls_d - Ls_q)(is_n^2 - i_d^2) - i_d^2(Ls_d - Ls_q)\right) = 0 \tag{26}$$

$$i_d^2 + \frac{\psi_f}{(Ls_d - Ls_q)} i_d - i_q^2 = 0 \tag{27}$$

Therefore, the d-axis current reference, in which the total driven torque has the maximum value, is calculated as,

$$i_d^* = \frac{-\psi_f}{2(Ls_d - Ls_q)} - \sqrt{\frac{\psi_f^2}{4(Ls_d - Ls_q)^2} + i_q^{*2}} \tag{28}$$

where i_q^*, i_q^* are the reference d-q axis currents. By using the reference value of the q-axis current which is obtained through the speed control loop, the command value of the d-axis current is calculated according to Eq. (28). It is important to note that the d-q axis inductances, Ls_d and Ls_q, in Eq. (28) are supposed to be constant, which is only valid for motors operating in the magnetic linear region. So if the machine operates in the magnetic saturation conditions, the d-q axis inductances are dependent to the d-q axis currents and are not constant. In these conditions, the values of the

Ls_d and Ls_q can be obtained from different current values depending on the motor load condition, which can be measured offline and saved into a look-up table (LUT).

4. Simulation and Experimental Results

Two processes are done to validate the theoretical concepts and evaluate the effectiveness of the proposed square wave injection method. At the first, the IPMSM sensorless control method is modeled and simulated in MATLAB. In the next step, one prototype IPM machine is tested. To simulate the proposed square wave injection method, MATLAB software is utilized to simulate the HF signal injection based sensorless techniques for a 4-poles IPM machine. Fig. 6 shows how the position error function can be built considering the rising-falling edge of the injected voltage and differentiation of the q-axis current. As shown, for $\Delta\theta = 0$, the q-axis induced current due to the d-axis HF injected voltage has a small amplitude close to zero. For the positive or negative position error, the amplitude of the q-axis induced current is considerable which can be used to generate the position error function at rising – falling edges of the injected voltage as mentioned in (17) and (18).

To evaluate the effectiveness of the proposed method, three commonly used HF injection methods, i.e., rotating sine wave injection in the stationary frame, pulsating sine wave injection, and pulsating square wave injection in the estimated synchronous frame are evaluated and compared with the proposed method. It should be noted that this comparison is done for those methods which use the carrier current as a function of the rotor position. Fig. 7(a) shows the dynamic performance of the proposed sensorless method in comparison to another HF injection based method in which the speed reference is given as +30, -30, and 0 rpm. Here, all of the PID coefficients are kept constant for a proper comparison. As shown, the proposed square wave injection method has a good dynamic response in terms of speed command and it also has a lower position error compared to others. Fig. 7(b-c) show the sensorless algorithm response to the sudden load disturbance. Total driven torque and d-q axis current considering the MTPA strategy are presented in this figure. As can be seen in the figure, the d-axis reference current is approximately zero in no-load conditions, as calculated according to the MTPA algorithm. It means that the reluctance torque component is zero. When the load is applied to the motor, MTPA algorithm produces the negative d-axis reference current that results in positive reluctance torque, which is then added to the electromagnetic torque to increase the resultant torque output to overcome the load torque. It should be noted that the d-axis feedback current has a high-frequency component due to the high frequency injected voltage on d-axis which can be removed by using a simple low pass

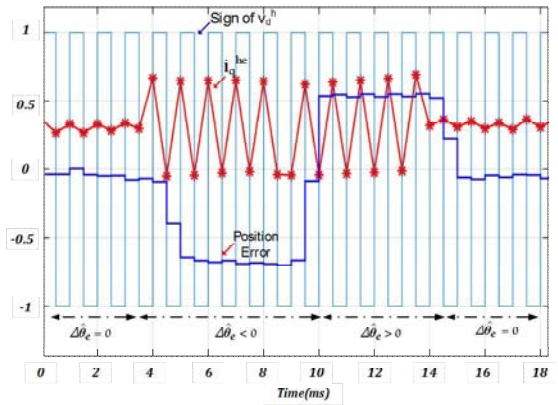

Fig. 6. Production of the position error function using the differentiation of the induced q-axis current

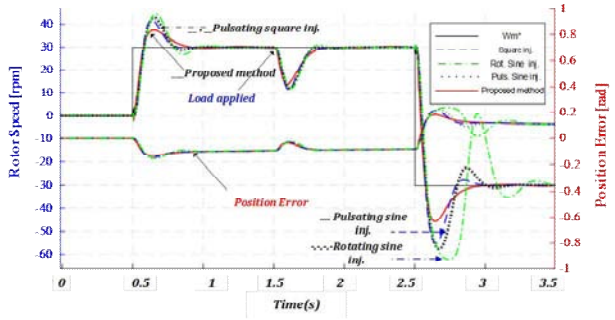

(a) Rotor speed and position error

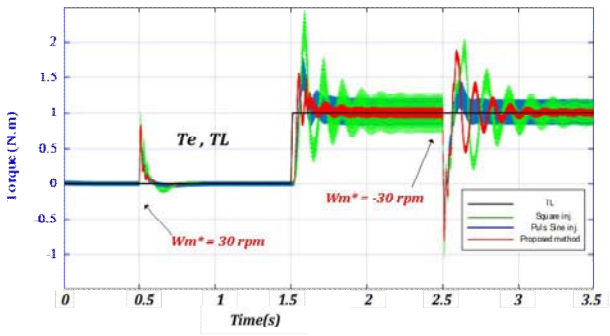

(b) Total driven torque

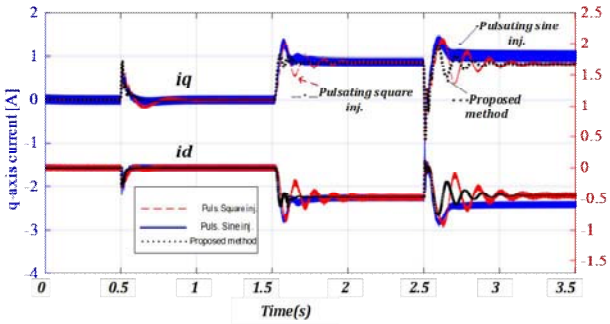

(c) d-q axis current considering the MTPA algorithm

Fig. 7. Comparison of the three commonly used current carrier based HF injection methods used in IPMSM sensorless drive with the proposed method

Table 2. IPM motor specification

IPM parameters	value	unit
Pole number	6	-
Rated current	2	A
d-axis inductance	122	mH
q-axis inductance	174	mH
Phase resistance	5.1	Ω
Rated speed	3000	Rpm
Rated voltage	220	V
Rated torque	1.5	Nm

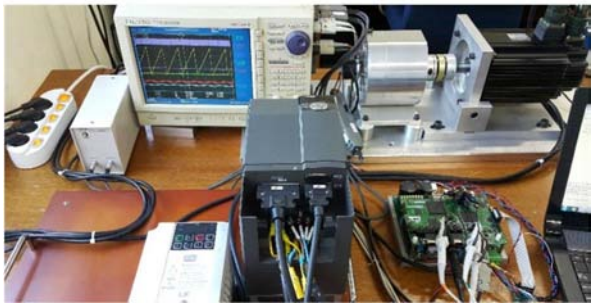

Fig. 8. Experimental test bench

filter. This figure also shows that the proposed method has a good performance in comparison to other methods.

To evaluate the performance of the proposed sensorless algorithm in a real condition, a hardware test bench is constructed based on a TMS320F2812 DSP board as the main signal processor. One intelligent power module which is used in the prototype inverter is FUJI 6MBP20RH. Both PWM frequency and current sampling frequency are set to 8 kHz and synchronized together by the software[23]. DC power supply for the inverter is 310 V.

Fig. 8 shows the experiment test bench. One AC servo motor is mechanically coupled to the IPM motor shaft to provide the necessary load. By adjusting the inverter operational mode to torque control mode, AC servo motor operates as the required load for IPMSM. To compare the actual rotor position with the estimated rotor position, one quadrature incremental encoder, 2500PPR, is mounted to the end of the motor shaft. The IPM motor parameters are specified in Table 2. Voltage magnitude and frequency of the injected square wave voltage is set to 20V/1kHz. To measure the phase currents two high accuracy shunt resistors, CSR2, are utilized as current sensor.

Fig. 9 shows the position error function for $+\Delta\theta$, 0, and $-\Delta\theta$. First, the rotor is aligned to the actual d-axis by applying the vector voltage V_{100}, which causes the motor to rotate and stop according to the axis of phase winding A. Then, HF voltage is injected into d-axis. In this position, by adding and subtracting the $\Delta\theta$ and considering the carrier q-axis current, the position error function can be generated. As can be seen in Fig. 9 the experiment result verifies the theoretical concepts as well as simulation result which was shown in Fig. 6.

To find the initial rotor position at standstill, the 20V/1KHz voltage is injected to the estimated d-axis at

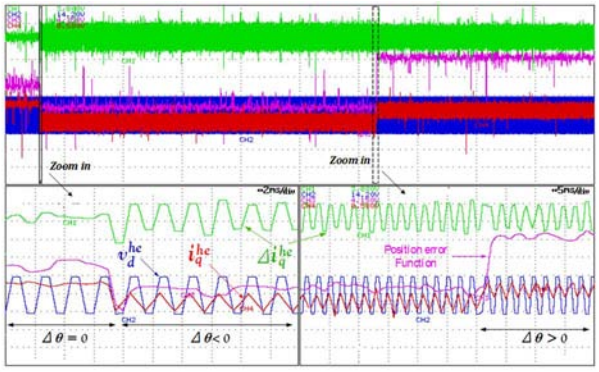

Fig. 9. Experimental result of the proposed method: production of the position error function

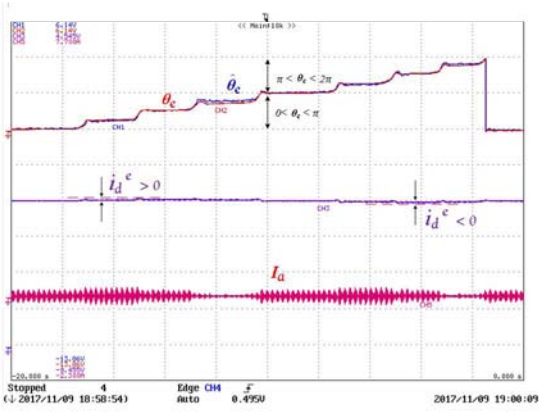

Fig. 10. Magnet polarity detection using the carrier d-axis current

zero current command on d-q axis ($i_d^* = 0$, $i_q^* = 0$). It should be noted that the initial rotor finding process consists of two processes. One for magnet polarity detection and another one for rotor position estimation. It should be noted that the rotor position near π rad is the maximum rotor position, at which the rotor can be located. Thus for rotor position which is bigger than π rad, the magnet polarity detection process is used to correct the estimated rotor position. Therefore, the initial rotor position can be obtained as,

$$\begin{cases} \hat{\theta}_e = \hat{\theta}_e & \text{if N pole was found} \\ \hat{\theta}_e = \hat{\theta}_e + \pi & \text{if S pole was found} \end{cases} \quad (29)$$

where $\hat{\theta}_e$ is the estimated rotor position considering the rotor magnet polarity. Fig. 10 shows the carrier d-axis current which is used for magnet polarity detection. As shown, the d-axis current has approximately positive values when the electrical rotor position is less than π rad and has negative values for rotor position bigger than π. By accumulating the values of the d-axis current for a short time, polarity of the magnet can be distinguished.

Unlike some conventional HF injection methods for sensorless control, the extra pulse voltage for magnet polarity detection is not needed in the proposed method.

Only one injection signal is used for both of position estimation and magnet polarity detection, which is beneficial for sensorless drive startup. Fig. 11 shows the initial rotor position in the initial state. To evaluate the effectiveness of the proposed method in the initial state, one comparison between the pulsating sine wave injection and the proposed method has been performed. It should be noted that the pulsating sine injection based on the negative carrier current has more merits compared to other negative current based HF injection methods such as rotating injection and etc. [21, 22].

As Fig. 11 shows, when the rotor is located near π rad, the proposed method is able to find the actual rotor position quickly in less than 50ms, while for HF sine wave injection method, this time is increased up to 145 ms. This results in a faster initial startup of IMPM sensorless drive. It should be noted that all of control parameters such as PID coefficients are kept constant for both injection methods to have a proper comparison.

Fig. 12 shows the initial state with 0, 50 and -50 rpm as the speed command profile. At the first, the drive is disabled. By starting the rotor finding process, the initial rotor position is found by considering the magnet polarity. The speed reference is set to 0, 50, -50 rpm and the rotor is able to rotate at the desired speed value. Fig. 13 shows the estimated rotor position, velocity, and position error when the speed reference is increased.

Fig. 14 shows the dynamic performance of the proposed method under load conditions. At the first, the speed reference is set to zero and at no load conditions, the speed reference is set to 60 rpm. The sudden load which is provided by the servomotor in torque mode control is applied to the IPM motor to evaluate the stability of the proposed method under the load condition. As can be seen from this figure, the proposed method is stable under load

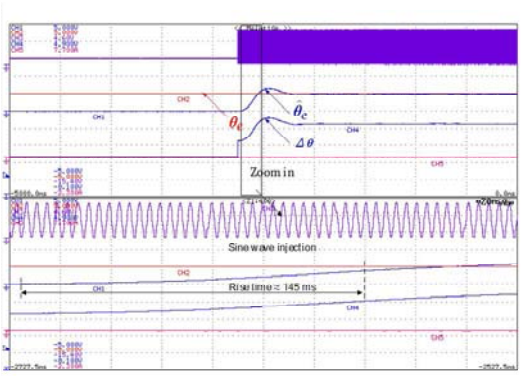

(a) Initial rotor position estimation using HF sine wave

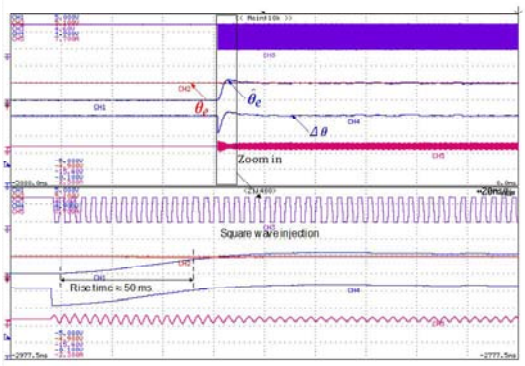

(b) Initial rotor position estimation using proposed HF square wave injection

Fig. 11. Initial rotor position at the initial state: (a) pulsating sine injection (b) proposed square wave injection

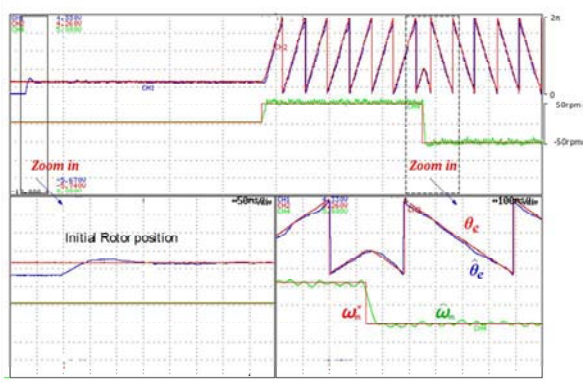

Fig. 12. Operation of the proposed method for initial rotor position and for 0, ± 50 rpm as a speed reference

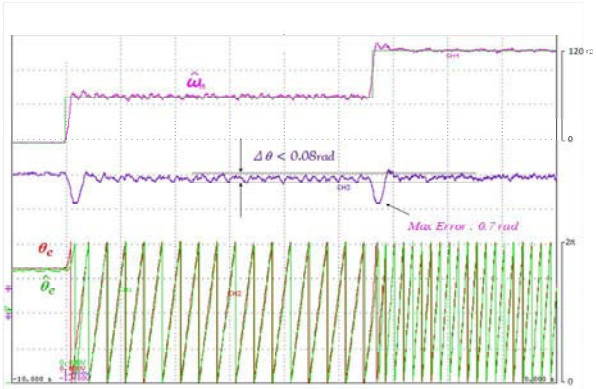

Fig. 13. Rotor position error, when the speed reference is increasing from 0, 60,120 rpm

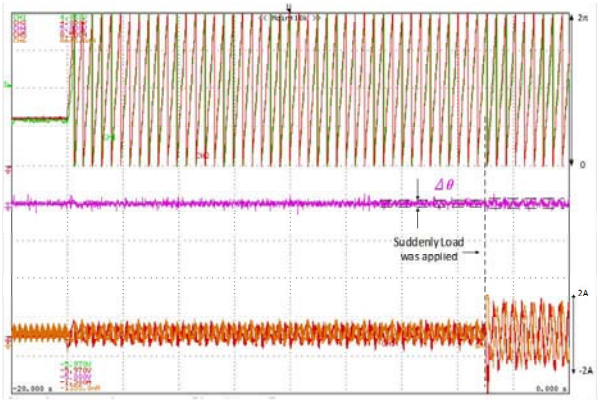

Fig. 14. Estimated rotor position, position error and phases current with and without load

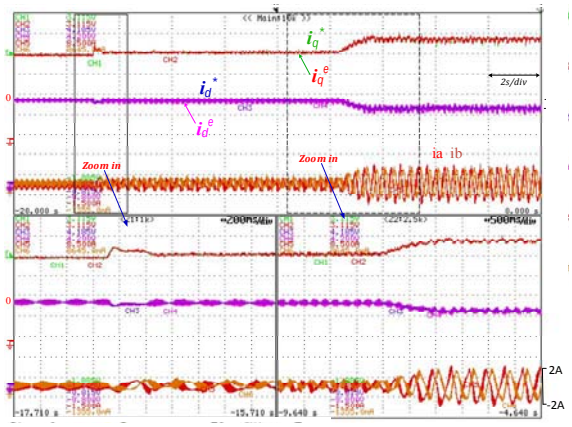

Fig.15. d-q axis current with MTPA strategy when the load is gradually increased

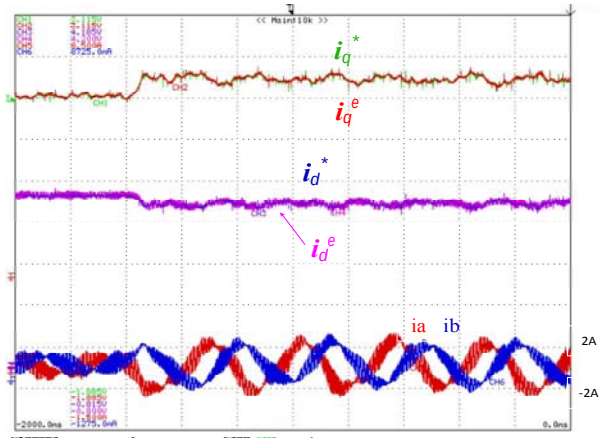

Fig.16. d-q axis currents with MTPA strategy when the load is suddenly increased

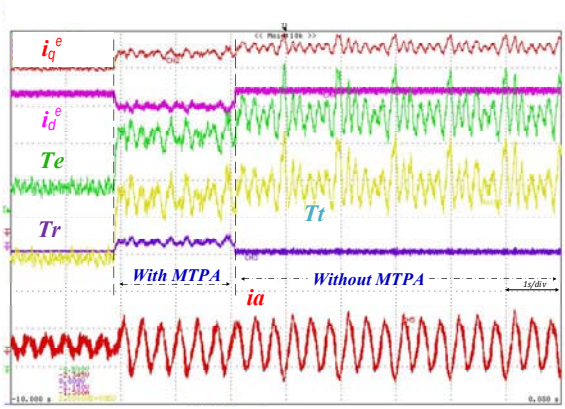

Fig.17. Electromagnetic, reluctance and total torque with and without MTPA strategy

operation although the position error is slightly increased.

Fig. 15 and 16 show the experiment results of the proposed method by taken into account the MTPA strategy, which is implemented in the proposed sensorless algorithm. Fig. 15 shows the d-q axis reference and feedback currents, in which q-axis reference current is generated by a speed loop and d-axis reference current is produced by MPTA algorithm. In this figure, the load is applied gradually to the IPMSM and the d-q axis reference current is followed as fast as possible, which can be seen in this figure. In the next test, a sudden load is applied to the motor. The d-q axis reference currents are generated by a speed loop and MTPA algorithm which has been shown in Fig. 16. It should be noted that the d-axis current has a high-frequency component due to the injected voltage on d-axis, which can be reduced by using a low pass filter. Fig. 14, 15 and 16 verify the validity of the proposed sensorless algorithm based on MTPA algorithm as well as the simulation results in Fig. 7. Fig. 17 shows the electromagnetic, reluctance, and driven torque of the IPMSM with and without the MTPA strategy. As can be seen, with the MTPA algorithm, the q-axis current has lower oscillation that results in lower electromagnetic torque ripple and consequently causes lower total torque ripple, which increases the stability of the proposed sensorless method.

5. Conclusion

In this paper, a high-frequency square wave voltage injection method for IMPSM sensorless control has been presented. Carrier induced q-axis current and d-axis current were used for position estimation and polarity detection. In the simulation and experiments, the estimated rotor position and speed were well kept in the actual values under various load conditions and speed reference, by using a simple PID controller. Concluded benefits of the proposed method have been described as bellow:

In the proposed method, a simple demodulation process based on the rising-falling edge of the injection voltage and induced q-axis current was used unlike sinusoidal injection methods and conventional square wave injection methods, which resulted in less processing time and improved sensorless control bandwidth.

The same injection voltage was used for both position estimation and magnet polarity detection which resulted in a fast search of initial rotor position. Moreover, a simple technique was used to find the magnet polarity which is important in the initial rotor position search process.

Instead of using the zero current command for the d-axis current control, MTPA algorithm based on the q-axis current reference and d-q axis inductances was utilized in order to improve the sensorless control performance.

Acknowledgements

This work was supported by "Human Resources Program in Energy Technology" of the Korea Institute of Energy Technology Evaluation and Planning(KETEP), granted financial resource from the Ministry of Trade, Industry & Energy, Republic of Korea (No. 20164010200940).

References

[1] Z. Q. Zhu and L. M. Gong, "Investigation of Effectiveness of Sensorless Operation in Carrier-Signal-Injection-Based Sensorless-Control Methods," *IEEE Transactions on Industrial Electronics*, vol. 58, issue 8, pp. 3431-3439, Aug. 2011.

[2] G. Wang, R. Yang, and D. Xu, "DSP-Based Control of Sensorless IPMSM Drives for Wide-Speed-Range Operation," *IEEE Transactions on Industrial Electronics*, vol. 60, issue 2, pp. 720-727, Feb. 2013.

[3] K. T. Chau, C. C. Chan, and C. Liu, "Overview of Permanent-Magnet Brushless Drives for Electric and Hybrid Electric Vehicles," *IEEE Transactions on Industrial Electronics*, vol. 55, issue 6,pp. 2246-2257, June 2008.

[4] T. D. Batzel and K. Y. Lee, "Slotless permanent magnet synchronous motor operation without a high resolution rotor angle sensor," *IEEE Transactions on Energy Conversion*, vol. 15, issue 4, pp. 366-371, December 2000.

[5] C. Zhiqian, M. Tomita, S. Doki, and S. Okuma, "An extended electromotive force model for sensorless control of interior permanent-magnet synchronous motors," *IEEE Transactions on Industrial Electronics*, vol. 50, issue 2, pp. 288-295, April 2003.

[6] S. Morimoto, K. Kawamoto, M. Sanada, and Y. Takeda, "Sensorless control strategy for salient-pole PMSM based on extended EMF in rotating reference frame," *IEEE Transactions on Industry Applications*, vol. 38, pp. 1054-1061, 2002.

[7] G. Wang, H. Zhan, G. Zhang, X. Gui, and D. Xu, "Adaptive Compensation Method of Position Estimation Harmonic Error for EMF-Based Observer in Sensorless IPMSM Drives," *IEEE Transactions on Power Electronics*, vol. 29, issue 6, pp. 3055-3064, June 2014.

[8] P. L. Xu and Z. Q. Zhu, "Novel Square-Wave Signal Injection Method Using Zero-Sequence Voltage for Sensorless Control of PMSM Drives," *IEEE Transactions on Industrial Electronics*, vol. 63, issue 12, pp. 7444-7454,Dec. 2016.

[9] W. Zine, L. Idkhajine, E. Monmasson, P. A. Chauvenet, A. Bruyere, and B. Condamin, "Investigation of saturation impact on an IPMSM saliency-based sensorless control for automotive applications," *in 2016 International Symposium on Power Electronics, Electrical Drives, Automation and Motion* (*SPEEDAM*), 2016, pp. 1238-1243.

[10] Z. Yue, Z. Zhe, M. Cong, W. Qiao, and Q. Liyan, "Sensorless control of surface-mounted permanent-magnet synchronous machines for low-speed operation based on high-frequency square-wave voltage injection," *in 2013 IEEE Industry Applications Society Annual Meeting*, 2013, pp. 1-8.

[11] Y. D. Yoon, S. K. Sul, S. Morimoto, and K. Ide, "High-Bandwidth Sensorless Algorithm for AC Machines Based on Square-Wave-Type Voltage Injection," *IEEE Transactions on Industry Applications*, vol. 47, issue 3, pp. 1361-1370, May- June 2011.

[12] Y. D. Yoon and S. K. Sul, "Sensorless Control for Induction Machines Based on Square-Wave Voltage Injection," *IEEE Transactions on Power Electronics*, vol. 29, issue 7, pp. 3637-3645, July 2014.

[13] S. C. Yang and Y. L. Hsu, "Full Speed Region Sensorless Drive of Permanent-Magnet Machine Combining Saliency-Based and Back-EMF-Based Drive," *IEEE Transactions on Industrial Electronics*, vol. 64, issue 2, pp. 1092-1101, Feb. 2017.

[14] P. L. Xu and Z. Q. Zhu, "Novel Carrier Signal Injection Method Using Zero-Sequence Voltage for Sensorless Control of PMSM Drives," *IEEE Transactions on Industrial Electronics*, vol. 63, issue 4, pp. 2053-2061, April 2016.

[15] P. L. Xu and Z. Q. Zhu, "Carrier Signal Injection-Based Sensorless Control for Permanent-Magnet Synchronous Machine Drives Considering Machine Parameter Asymmetry," *IEEE Transactions on Industrial Electronics*, vol. 63, issue 5, pp. 2813-2824, May 2016.

[16] J. M. Liu and Z. Q. Zhu, "Novel Sensorless Control Strategy With Injection of High-Frequency Pulsating Carrier Signal Into Stationary Reference Frame," *IEEE Transactions on Industry Applications*, vol. 50, issue 4,pp. 2574-2583,July-Aug. 2014.

[17] N. Bianchi, S. Bolognani, J. H. Jang, and S. K. Sul, "Advantages of Inset PM Machines for Zero-Speed Sensorless Position Detection," *IEEE Transactions on Industry Applications*, vol. 44, issue 4, pp. 1190-1198, July-Aug. 2008.

[18] M. Linke, R. Kennel, and J. Holtz, "Sensorless speed and position control of synchronous machines using alternating carrier injection," *in Electric Machines and Drives Conference, 2003. IEMDC'03. IEEE International*, vol. 2, pp. 1211-1217, 2003.

[19] Y. C. Kwon and S. K. Sul, "Reduction of Injection Voltage in Signal Injection Sensorless Drives Using a Capacitor-Integrated Inverter," *IEEE Transactions on Power Electronics*, vol. 32,issue 8, pp. 6261-6274, Aug. 2017.

[20] S. Amornwongpeeti, O. Kiselychnyk, J. Wang, N. Shah, and M. Soumelidis, "Speed control of IPMSM motor drives using Model Reference Adaptive technique," *in 2017 International Conference on Applied System Innovation(ICASI)*, pp. 672-675, 2017.

[21] P. L. Xu and Z. Q. Zhu, "Comparison of carrier signal injection methods for sensorless control of PMSM drives," *in 2015 IEEE Energy Conversion Congress and Exposition (ECCE)*, pp. 5616-5623, 2015.

[22] A. Ahmadreza, L. Dong-Hee, A. Jin-Woo, and N. Sayed Morteza Saghaeian, "Comparison of High Frequency Square Wave and Sinusoidal Wave Signal

Injection Methods for IPMSM Sensorless Drive Application," pp. 704-706, 2017.
[23] F. Briz, M. W. Degner, P. Garcia, and J. M. Guerrero, "Rotor position estimation of AC machines using the zero-sequence carrier-signal voltage," *IEEE Transactions on Industry Applications*, vol. 41, issue 6, pp. 1637-1646, Nov.-Dec. 2005.
[24] M. E. Haque, Z. Limin, and M. F. Rahman, "A sensorless initial rotor position estimation scheme for a direct torque controlled interior permanent magnet synchronous motor drive," *IEEE Transactions on Power Electronics*, vol. 18, issue 6, pp. 1376-1383, Nov. 2003.
[25] L. M. Gong and Z. Q. Zhu, "Robust Initial Rotor Position Estimation of Permanent-Magnet Brushless AC Machines With Carrier-Signal-Injection-Based Sensorless Control," *IEEE Transactions on Industry Applications*, vol. 49, issue 6, pp. 2602-2609, Nov.-Dec. 2013.
[1] Z. Q. Zhu and L. M. Gong, "Investigation of Effectiveness of Sensorless Operation in Carrier-Signal-Injection-Based Sensorless-Control Methods," *IEEE Transactions on Industrial Electronics*, vol. 58, pp. 3431-3439, 2011.
[2] G. Wang, R. Yang, and D. Xu, "DSP-Based Control of Sensorless IPMSM Drives for Wide-Speed-Range Operation," *IEEE Transactions on Industrial Electronics*, vol. 60, pp. 720-727, 2013.
[3] K. T. Chau, C. C. Chan, and C. Liu, "Overview of Permanent-Magnet Brushless Drives for Electric and Hybrid Electric Vehicles," *IEEE Transactions on Industrial Electronics*, vol. 55, pp. 2246-2257, 2008.
[4] T. D. Batzel and K. Y. Lee, "Slotless permanent magnet synchronous motor operation without a high resolution rotor angle sensor," *IEEE Transactions on Energy Conversion*, vol. 15, pp. 366-371, 2000.
[5] C. Zhiqian, M. Tomita, S. Doki, and S. Okuma, "An extended electromotive force model for sensorless control of interior permanent-magnet synchronous motors," *IEEE Transactions on Industrial Electronics*, vol. 50, pp. 288-295, 2003.
[6] S. Morimoto, K. Kawamoto, M. Sanada, and Y. Takeda, "Sensorless control strategy for salient-pole PMSM based on extended EMF in rotating reference frame," *IEEE Transactions on Industry Applications*, vol. 38, pp. 1054-1061, 2002.
[7] G. Wang, H. Zhan, G. Zhang, X. Gui, and D. Xu, "Adaptive Compensation Method of Position Estimation Harmonic Error for EMF-Based Observer in Sensorless IPMSM Drives," *IEEE Transactions on Power Electronics*, vol. 29, pp. 3055-3064, 2014.
[8] P. L. Xu and Z. Q. Zhu, "Novel Square-Wave Signal Injection Method Using Zero-Sequence Voltage for Sensorless Control of PMSM Drives," *IEEE Transactions on Industrial Electronics*, vol. 63, pp. 7444-7454, 2016.
[9] W. Zine, L. Idkhajine, E. Monmasson, P. A. Chauvenet, A. Bruyere, and B. Condamin, "Investigation of saturation impact on an IPMSM saliency-based sensorless control for automotive applications," *in 2016 International Symposium on Power Electronics, Electrical Drives, Automation and Motion* (*SPEEDAM*), 2016, pp. 1238-1243.
[10] Z. Yue, Z. Zhe, M. Cong, W. Qiao, and Q. Liyan, "Sensorless control of surface-mounted permanent-magnet synchronous machines for low-speed operation based on high-frequency square-wave voltage injection," *in 2013 IEEE Industry Applications Society Annual Meeting*, 2013, pp. 1-8.
[11] Y. D. Yoon, S. K. Sul, S. Morimoto, and K. Ide, "High-Bandwidth Sensorless Algorithm for AC Machines Based on Square-Wave-Type Voltage Injection," *IEEE Transactions on Industry Applications*, vol. 47, pp. 1361-1370, 2011.
[12] Y. D. Yoon and S. K. Sul, "Sensorless Control for Induction Machines Based on Square-Wave Voltage Injection," *IEEE Transactions on Power Electronics*, vol. 29, pp. 3637-3645, 2014.
[13] S. C. Yang and Y. L. Hsu, "Full Speed Region Sensorless Drive of Permanent-Magnet Machine Combining Saliency-Based and Back-EMF-Based Drive," *IEEE Transactions on Industrial Electronics*, vol. 64, pp. 1092-1101, 2017.
[14] P. L. Xu and Z. Q. Zhu, "Novel Carrier Signal Injection Method Using Zero-Sequence Voltage for Sensorless Control of PMSM Drives," *IEEE Transactions on Industrial Electronics*, vol. 63, pp. 2053-2061, 2016.
[15] P. L. Xu and Z. Q. Zhu, "Carrier Signal Injection-Based Sensorless Control for Permanent-Magnet Synchronous Machine Drives Considering Machine Parameter Asymmetry," *IEEE Transactions on Industrial Electronics*, vol. 63, pp. 2813-2824, 2016.
[16] J. M. Liu and Z. Q. Zhu, "Novel Sensorless Control Strategy With Injection of High-Frequency Pulsating Carrier Signal Into Stationary Reference Frame," *IEEE Transactions on Industry Applications*, vol. 50, pp. 2574-2583, 2014.
[17] N. Bianchi, S. Bolognani, J. H. Jang, and S. K. Sul, "Advantages of Inset PM Machines for Zero-Speed Sensorless Position Detection," *IEEE Transactions on Industry Applications*, vol. 44, pp. 1190-1198, 2008.
[18] M. Linke, R. Kennel, and J. Holtz, "Sensorless speed and position control of synchronous machines using alternating carrier injection," *in Electric Machines and Drives Conference, 2003. IEMDC'03. IEEE International*, vol. 2, pp. 1211-1217, 2003.
[19] Y. C. Kwon and S. K. Sul, "Reduction of Injection Voltage in Signal Injection Sensorless Drives Using a Capacitor-Integrated Inverter," *IEEE Transactions on Power Electronics*, vol. 32, pp. 6261-6274, 2017.
[20] S. Amornwongpeeti, O. Kiselychnyk, J. Wang, N.

Shah, and M. Soumelidis, "Speed control of IPMSM motor drives using Model Reference Adaptive technique," *in 2017 International Conference on Applied System Innovation(ICASI)*, pp. 672-675, 2017.
[21] P. L. Xu and Z. Q. Zhu, "Comparison of carrier signal injection methods for sensorless control of PMSM drives," *in 2015 IEEE Energy Conversion Congress and Exposition (ECCE)*, pp. 5616-5623, 2015.
[22] A. Ahmadreza, L. Dong-Hee, A. Jin-Woo, and N. Sayed Morteza Saghaeian, "Comparison of High Frequency Square Wave and Sinusoidal Wave Signal Injection Methods for IPMSM Sensorless Drive Application," pp. 704-706, 2017.
[23] F. Briz, M. W. Degner, P. Garcia, and J. M. Guerrero, "Rotor position estimation of AC machines using the zero-sequence carrier-signal voltage," *IEEE Transactions on Industry Applications*, vol. 41, pp. 1637-1646, 2005.
[24] M. E. Haque, Z. Limin, and M. F. Rahman, "A sensorless initial rotor position estimation scheme for a direct torque controlled interior permanent magnet synchronous motor drive," *IEEE Transactions on Power Electronics*, vol. 18, pp. 1376-1383, 2003.
[25] L. M. Gong and Z. Q. Zhu, "Robust Initial Rotor Position Estimation of Permanent-Magnet Brushless AC Machines With Carrier-Signal-Injection-Based Sensorless Control," *IEEE Transactions on Industry Applications*, vol. 49, pp. 2602-2609, 2013.

Ahma dreza Alaei He received B.S degree in electrical engineering from Isfahan university of Technology, Isfahan, Iran, in 2004 and the M.S. degree in electrical engineering from the Khaje Nasir Toosi University (KNTU), Tehran, in 2006. Here he is currently working toward the Ph.D. degree in power electronics and electrical drives. His current research interests include parameter identification technique, and control of electrical drives, with main focus on sensorless field-oriented control of interior permanent magnet synchronous motor.

Dong-Hee Lee He was born on Nov. 11, 1970 and received his B.S, M.S., and Ph. D degrees in Electrical Engineering from Pusan National University, Pusan, Korea in 1996, 1998, and 2001, respectively. He worked as a Senior Researcher of Servo R&D Team at OTIS-LG, from 2002 to 2005. He has been with Kyungsung University, Pusan, Korea as an Assistant professor in the Department of Mechatronics Engineering since 2005. He has been the Director of the Advance Electric Machinery and Power Electronics Center since 2009. His major research field is Power Electronics and motor control system.

Jin-Woo Ahn He was born in Busan, Korea, in 1958. He received his B.S., M.S., and Ph.D. degrees in Electrical Engineering from Pusan National University, Busan, Korea, in 1984, 1986 and 1992, respectively. He has been with Kyungsung University, Busan, Korea, as a professor in the Department of Mechatronics Engineering since 1992. He is Vice President of KIEE and the director of the Smart Mechatronics Advanced Research and Technology Institute and Senior Easy Life RIS Center. He is the author of five books including SRM, the author of more than 200 papers and has more than 30 patents. His current research interests are advanced motor drive systems and electric vehicle drives. He also received many awards from IEEE, KIEE and KIPE and including Order of Science and Technology Merit from the President of the Republic of Korea for his numerous contributions for the electrical engineering. He served as a Conference Chairman of International Conference on Electric Machines and Systems2013 (ICEMS 2013), and of International Conference on Industrial Technology 2014 (IEEE/ICIT2014) and serving as a Conference Chairman of IEEE Transportation Electrification Conference and Expo 2016 Busan (ITEC2016 Busan). He is a Fellow of the Korean Institute of Electrical Engineers, a member of the Korean Institute of Power Electronics and a Senior member of the IEEE.

Sayed Morteza Saghaeian Nejad He received his B.S, M.S, and Ph.D. degrees in Electrical and Computer Engineering Department, University of Kentucky, USA, in 1975, 1977, and 1989, respectively. Since 1979, he has been a faculty member of Isfahan University of Technology, where he is currently a Professor in electrical and computer engineering department. He is the author or coauthor of various journal and conference papers. His research interests include analysis and control of electrical machines, control of electrical drives, power electronics, and switched reluctance machines.